Research on Engineering Structures & Materials
www.jresm.org
MIM Research Group

Research Article

Investigation of the corrosion behavior and bioactivity of TI6AL4V alloy coated with bio-composite powders in simulated body fluid

Rusul S. Hadi [a], Hanaa A. Al-Kaisy [*,b], Mohanad N. Al-Shroofy [c]

Department of Materials Engineering, University of Technology, Baghdad, Iraq

Article Info

Article History:

Received 12 Apr 2026

Accepted 04 June 2026

Keywords:

Electrostatic spray method;
Polylactic Acid (PLA);
ZrO_2 and CeO_2 particles;
Bio-composite coating

Abstract

This study investigates the effect of incorporating ZrO_2 and CeO_2 particles on the corrosion resistance of Ti6Al4V alloy for knee implant applications in simulated body fluid (SBF) at 37 °C. PLA-based coatings were reinforced with 9 wt.% and 15 wt.% of CeO_2 and ZrO_2 particles. alongside a control coating of 100 wt% PLA. The coatings were applied using the Electrostatic Spray Deposition (ESD) technique. Surface morphology analysis using SEM/EDS revealed the accumulation of calcium and phosphorus within the coatings, indicating enhanced bioactivity and strong bonding potential with surrounding bone tissue. Scratch hardness testing demonstrated improved adhesion and the formation of a protective layer compared to uncoated titanium alloy. Electrochemical behavior was evaluated using the potentiostatic method, including Tafel slope analysis, corrosion rate (mm/y), and polarization resistance (Rp). Results showed a significant reduction in corrosion current density and corrosion rate with the addition of ceramic particles. Notably, the corrosion rates reached 0.001552 mm/y for (PLA + 15% ZrO_2) and 1.901×10^{-6} mm/y for (PLA + 15% CeO_2), compared to 0.34109 mm/y for uncoated titanium alloy, confirming the effectiveness of the composite coatings.

1. Introduction

The skeletal system, of which cortical bone constitutes a significant portion (approx. 15% of body weight), is a fundamental structural component. Bone tissue has a two-layered structure: the outer layer, known as cortical bone, comprises about 80% of the total bone mass in adults and has a low porosity of 3% to 5%. [1]. About 70–80% of medical implants are formed utilizing metallic biomaterials. These materials are usually used in orthopedics for applications such as bone healing, fracture fixation, and load support. Widely used metallic biomaterials include 316L stainless steel, 304L stainless steel, titanium, titanium-nickel alloys, cobalt-based alloys (e.g., Co-Cr-Mo), and other metal-based materials [4, 5]. The study has primarily focused on titanium alloys, with particular emphasis on Ti-6Al-4V. This focus is mainly due to titanium alloys becoming the favored material for various modern medical and dental applications. Ti-6Al-4V, in particular, is known for its excellent corrosion resistance, low toxicity, high biocompatibility, excellent mechanical properties, chemical stability, and relatively low Young's modulus. These characteristics have led to its wide use in orthopedic surgery [6,7]. After exposure to air, titanium alloys form a stable oxide layer on their surface, which enhances their bone-bonding properties when used in implants. This unique corrosion resistance is due to the passive film formed on the alloy's surface. To achieve positive integration of implants with bone tissue, surface characterization of bone implants plays an important role. several challenges associated with titanium-based implants (Ti6Al4V), counting the emission of harmful ions as vanadium also aluminum, inadequate corrosion resistance, stress

*Corresponding author: b10769@uotechnology.edu.iq
[a]orcid.org/0000-0002-2362-2588; [b]orcid.org/0000-0002-9052-4451; [c]orcid.org/0000-0002-3902-8575
DOI: http://dx.doi.org/10.17515/resm2026-1610ma0412rs

shielding results, also suboptimal osseointegration. Moreover, issues for example abrasive corrosion also bacterial colonization are evaluated because of their potential impact on the long-term viability of implants, prompting the exploration of alternative materials and surface enhancements. [8,9]. Physical and mechanical modifications, such as the addition of manufacturing, subtractive methods, and laser treatments, cause variation in the surface properties of Titanium alloys at both macroscopic and microscopic scales [10]. Techniques such as physical vapor deposition, sandblasting, and laser ablation are typically used to enhance tissue integration by modifying surface topography, increasing roughness, or applying mechanical and physical coatings [11,12]. Chemical modification includes incorporating substances or showing specific chemical reactions on the implant's surface. Processes such as electrophoretic deposition (EPD), anodic oxidation, and chemical vapor deposition (CVD) are used to modify the surface chemistry. These methods enhance bioactivity and also promote improved interactions with the surrounding tissue [13]. Biological coating fusion involves applying biologically active chemicals or substances to modify an implant's composition and surface structure, thereby conferring specific biological functionalities [14]. The integration of multifunctional or double-purpose coatings, achieved through smart coating design, enables distinct functionalities across regions or within gradient variations [15]. Additionally, this process effectively merges antibacterial properties amongst bone-growth-promoting features. The appropriate surface modification is guided by the implant's intended use, the required biological response, and the expected mechanical properties [16]. C. Zhao et al. (2020) utilized multi-arc ion plating to deposit TiN and Ti/TiN multilayer coatings onto the surface of the Ti6Al4V alloy. The findings showed that the tribo-corrosion resistance of the multilayered coatings was enhanced twofold compared with the uncoated Ti6Al4V alloy and the single TiN coating after immersion in simulated body fluid at 37°C [17]. In 2021, Ghofran Dhafer et al. used the electrostatic deposition technique to improve the surface of the 316L stainless steel (SS) substrate by employing a bio composite coating derived from a PMMA-based composite with various hydroxyapatite concentrations. The surface morphology and phase composition of the coatings were measured using FTIR and FESEM/EDS methods. Moreover, the coated specimens were assessed for biological performance by analyzing their wettability and Osseo conductivity properties. The findings showed that the coating adhered uniformly to the 316L SS substrate, resulting in a notable enhancement in the alloy's biocompatibility and biological activity [18]. S. Bashar et al. utilized the electrostatic spray method to coat pure titanium substrates throughout varying proportions of hydroxyapatite (HAP) mixed with nickel oxide (NiO)and PMMA. Surface analysis done using FESEM/EDS and XRD shown homogeneous, identical, and crack-free coatings along with enhanced surface wettability a important factor for biomedical implants [19]. G.Y. Atay et. al., Recent studies have also explored the integration of antibacterial agents, such as nano Ag particles, into Ti6Al4V alloys to prevent implant-related infections. First, Ti-6Al-4 V titanium alloys were made through the powder metallurgy process. The chief purpose of this paper, antibacterial study against Escherichia Coli and Staphylococcus Aureus was presented through percentage reduction exam. While the coating process was shown to be additional positive in antibacterial analyses, the whole Nano Ag application functioning was created to be larger against Escherichia Coli bacteria. It was observed that the sample containing 5% Nano-Ag exhibited a 100% antibacterial effect against both E. coli and S. aureus [20]. S. V. Harb et. al. (2024), The development of customized implants by additive manufacturing has considerably advanced the field of personalized medicine. In this paper, a 3D-printed bioabsorbable composite made of poly(lactic acid) (PLA) and β-tricalcium phosphate (TCP) with a 10% weight composition was improved with cerium oxide nanoparticles (CeNPs) at concentrations of 1, 5, also 10 wt % for bone repair purposes[21].

The difference between this study the electrostatic deposition process was used to enhance the surface of a titanium alloy (Ti6Al4V) substrate by applying a bio composite coating resulting from a PLA-based composite reinforced by many ZrO2 and CeO2 ratios. The studies proved that the coating layer adhered homogeneously to the Ti6Al4V substrate, The dispersed nanoparticles in the PLA successfully fill the micro-voids also pores existing in the pure polymer. This filling blocks and reduce the penetration of corrosive ions (for example chloride ions ,oxygen ,and moisture) to the underlying titanium alloy surface through making a highly tortuous path oxides have very high also thermal stability in aggressive corrosive environments [22,23].

In this study, the ESD approach was used to apply PLA, ZrO2/PLA, and CeO2/PLA bio-composite coatings onto the Ti6Al4V substrate, aiming to enhance both the biocompatibility and corrosion resistance of the coating alloy.

2. Materials and Methods

A Titanium alloy (Ti6Al4V) rod was cut into a specimen using wire-cut EDM. The chemical composition of Ti6Al4V contains Ti (89.802%), Al (6%), V (4%), O (0.08%), Fe (0.07%), C (0.03%), N (0.01%), and H (0.008%). When cutting, the samples were wet-ground with SiC sandpaper grits of 100, 150, and 200 grit to increase the substrate's surface roughness to increase mechanical interlocking for the coating. Next, the samples were cleaned and sequentially rinsed with deionized water and methanol alcohol. They were then air dried completely and was stored in a desiccator to ensure dryness. In the next step, the prepared samples under microstructural testing and were studied in a body fluid mimicking environment (SBF) ISO23317). This was achieved through mixing about 1000 mL of distilled water with the SBF powder in a glass beaker, utilizing a stirring rod to ensure full mixing. The beaker was then put on a magnetic stirrer and covered by plastic or glass film. Finally, the mixture was stirred for one hour at a organized temperature of 37 ± 1 °C.

Titanium alloy (Ti6Al4V) produce by (XI'AN FUNCTION MATERIAL GROUP CO.,LTD) China, Polylactic acid (PLA) is the base material resulting from "Luminy LX175 has purity about (96)% with particle size(53)nm and molecular weight(50,000 - 150,000 g/mol)g/mol and glass transition temperature (60)C_0 with different types of ceramic particles, zirconium oxide (ZrO_2) was obtained from (LUXION company ,Registered in England & Wales), has purity about (99.5)% with particle size(65)nm , cerium oxide(CeO_2) it is purchased from (SIGMA-ALDRICH, St. Louis, MO, USA)featuring an average particle size of (50 nm) also a purity level of approximately 99.9% .that were used to produce composite

Table 1. Chemical Composition of simulated bodily fluid

The regents used	$NaSo_4$ (g)	$MgCl_2.6H_2O$(g)	$K_2HPO_4.3H_2O$	$NaHCO_3$ (g)	KCl (g)	$CaCl_2$ (g)	NaCl (g)	HCl (g)
simulated bodily fluid	0,072	0,311	0,231	0,355	0,225	0,292	8,035	39

3. Composite Coating Preparations

A polymeric coating based on polylactic acid (PLA) was developed with CeO_2 and ZrO_2 bioactive ceramic particles at varying weight percentages (9, and 15 wt%) as reinforcements. These components are placed inside a container and mixed and blending by dry mechanical mixing for 30 minutes to confirm a uniform mixture suitable for coating applications. The mass percentages of CeO_2 and ZrO_2 to PLA in the three different types of composite powders were 9:91, and 15:85, respectively. The Electrostatic Spray Deposition (ESD) system includes a stainless-steel capillary nozzle joined to a high-voltage power source by positive polarity (COLO CL668W/30kV/PN) and uses a metallic substrate holder for material deposition. To control the thickness of the deposited layer, the voltage was adjusted to 25 kV, with a fixed gap of 15 cm between the substrate and the spray gun. The spraying method lasted for 30 seconds. After deposition, the coated specimen underwent heat treatment in an electric furnace at 160°C for 30 minutes to finalize the coating process, after three to four times the experiments were repeated a temperature of 160°C was chosen to increase inter-particle diffusion), since after a period of time, the sample becomes electrically uncharged, causing the powder to fall off and the coating to fail. So, a partial melting of the PLA occurs after the addition of ceramic particles, because below this temperature the powder oxidizes, resulting in coating failure and Above 160°C, the powder burns and the coating fails.as showed in Fig. 1.

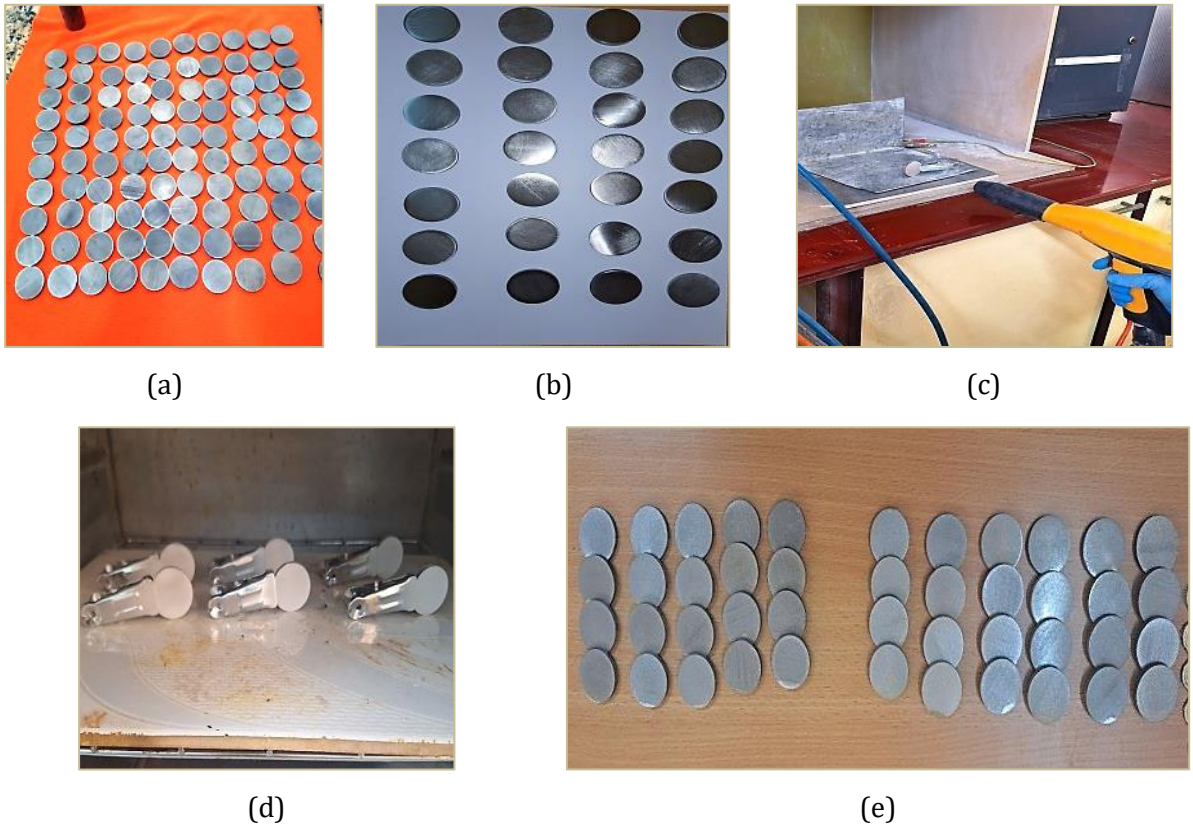

Fig. 1. (a) samples before cleaning,(b) samples after cleaning,(c) coating process ,(d) curing in the oven ,(e) coated samples

4. Results and Discussion

4.1 Morphological Analysis (FESEM)

The SEM images of PLA, PLA/ ZrO_2, and PLA/ CeO_2 composite coatings, produced with several concentrations of PLA, CeO_2, and ZrO_2, are shown in Fig. 2. The PLA coating exhibits an ideal structure, characterized as a uniform porous film, consistent with the findings reported in references [24], which describe similar electrostatically deposited PLA coatings. All samples demonstrate that the implant surfaces were uniformly coated with smooth, crack-free layers exhibiting strong adhesion. The cross-sectional images of the coating samples, shown in Fig. 2.(d), indicate an uniform deposition of the coating layer and uniform integration and distribution of ceramic particles within the PLA matrix. It demonstrates a balanced level of porosity without significant cracks, creating promising conditions for osseointegration. In particular, despite partial melting of PLA particles during the heating technique used in film production, they retained their spherical shape during deposition and curing.

The morphology of these coated films gives promising corrosion resistance. The presence of microscopic pores within the coatings, attributed to the addition of ZrO_2 and CeO_2, enhances cell adhesion. Fig.3 of EDS test by (TESCAN Vega II XMU) system. highlights the presence of elements on the surface (Carbon, Oxygen, Titanium, Zirconium, Cerium, etc.)

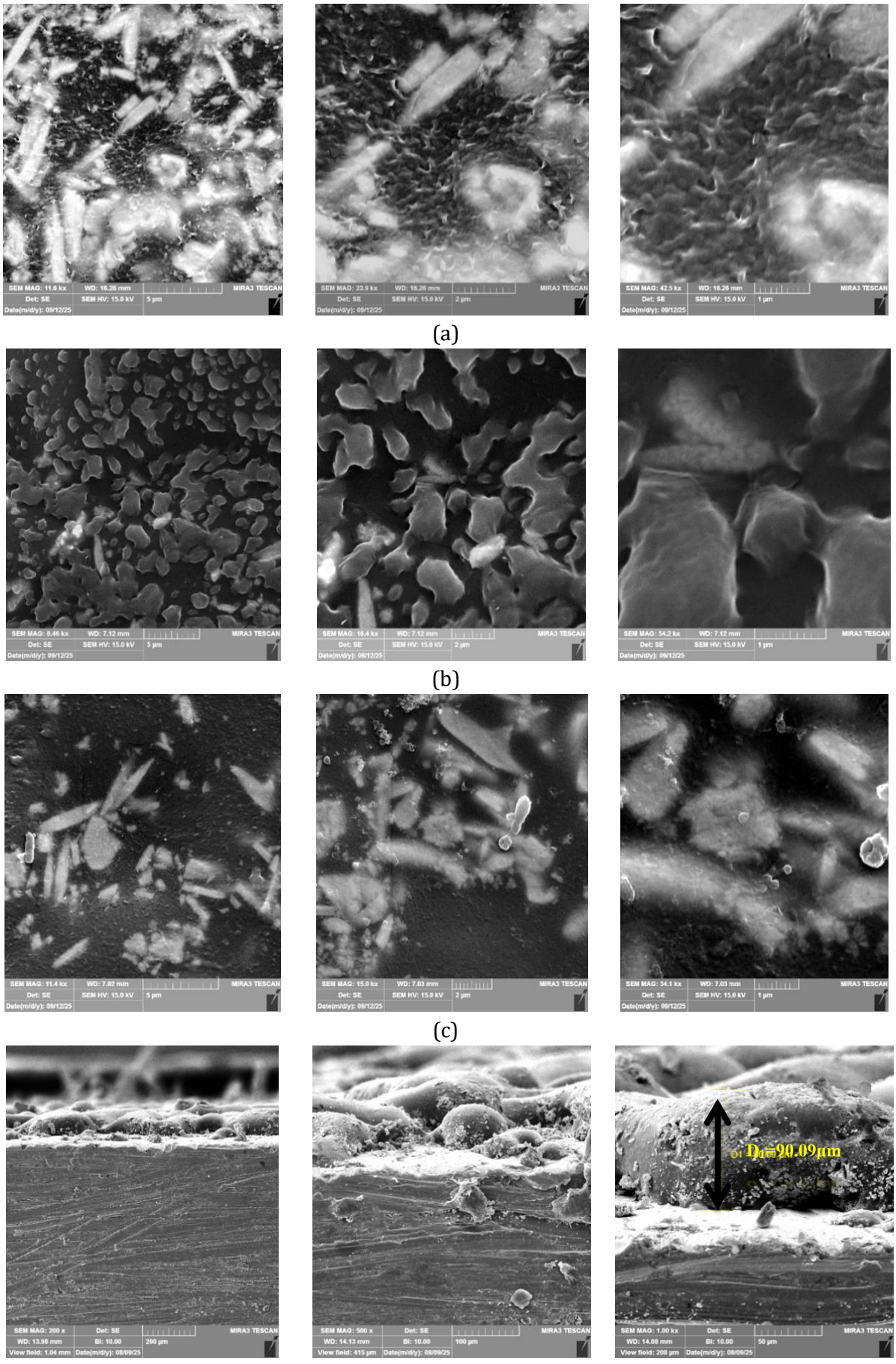

Fig. 2. FESEM of coated specimen before immersed in SBF solution of (a) PLA, (b)PLA 9%ZrO_2, (c) PLA+9%CeO_2, (d) cross-section thickness images of the coating samples

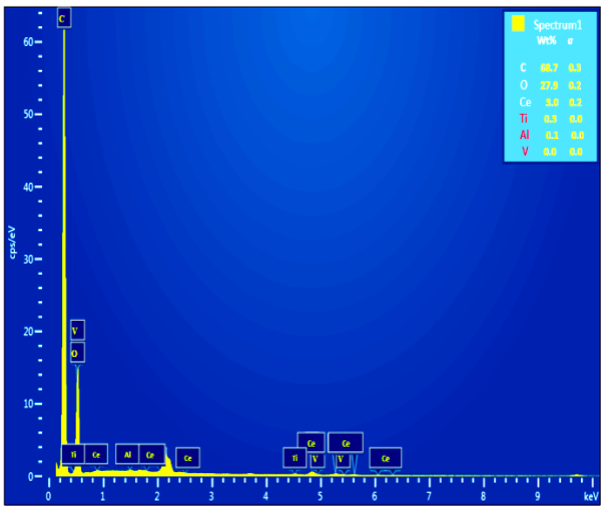

(a)

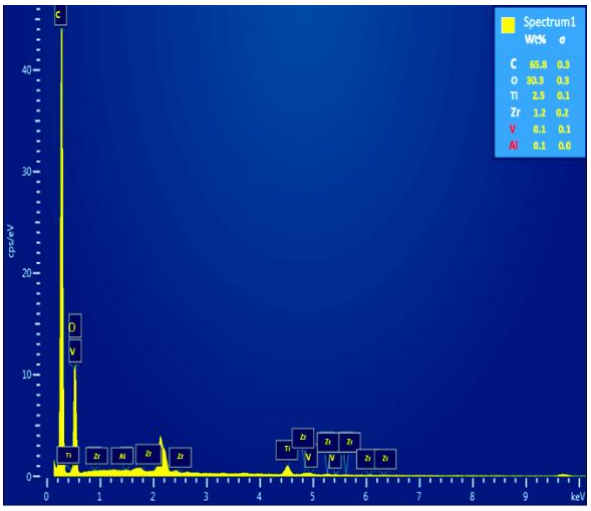

(b)

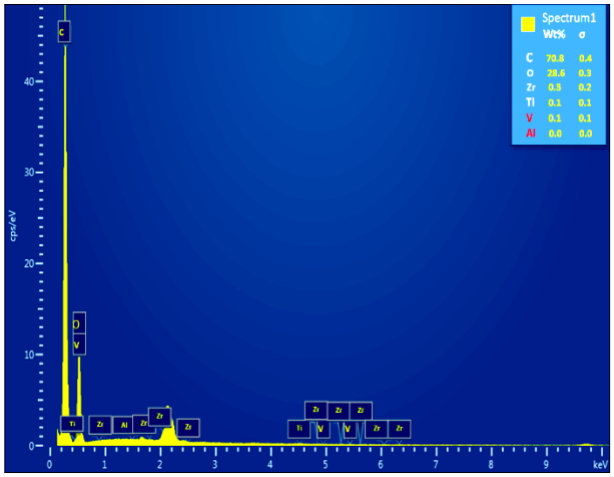

(c)

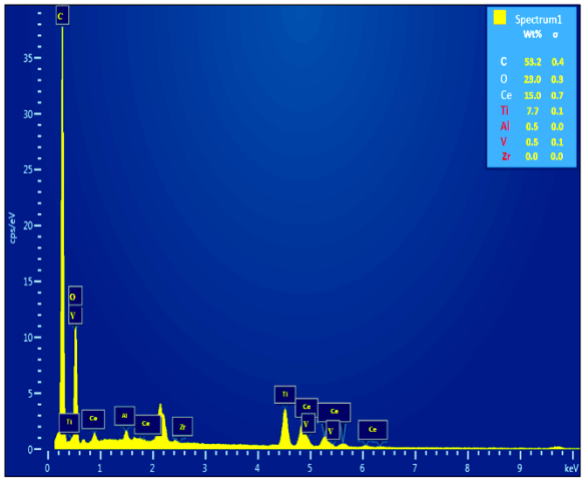

(d)

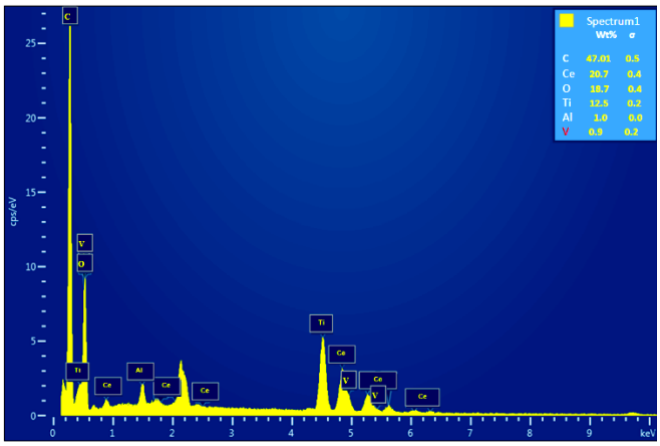

(e)

Fig. 3. EDS test of coated samples of (a) PLA, (b)PLA+9% ZrO_2, (c)PLA + 15% ZrO_2, (d) PLA+9%CeO_2, (e) PLA+15%CeO_2

4.2 Osseointegration Potential

Osteo-conductivity levels are important for evaluating the functioning of bone implants. These levels significantly help maintain a stable mechanical connection between the implant and the implantation site by promoting a strong, permanent bond with the surrounding bone tissue [25]. To measure this property, the in vitro bioactivity of covered samples was studied. The analysis aimed to determine the formation of a layer on the implant surface coated with specific biomaterials during immersion in simulated body fluid (SBF). Coated samples were immersed in SBF for 21 days to examine this method. The creation layers were closely tested utilizing FESEM. Fig. 1 shows the results for the CeO2/PLA- and ZrO2/PLA-coated samples, which were prepared by Electrostatic Spray Deposition (ESD). This technique results in a homogeneous distribution of cerium and zirconium particles, forming clusters on the sample surfaces without any indication of agglomeration. The EDS test in Fig. 2 before immersed in simulated body fluid (SBF) presented no amount of calcium (Ca) and phosphorus (P). When specimens are immersed in simulated body fluid (SBF) at 37°C, chemical reactions, for example, spontaneous precipitation, promote the growth of a surface layer. It is believed that the material's functional groups, along with its surface chemistry, play an important role in enhancing its bonding with bone as shows in Fig. 4 The results from the composite-coated samples from the EDS test in Fig. 5 show presented calcium (Ca) and phosphorus (P) creation after immersion in SBF, representative enhanced apatite formation from calcium (1.3) % and phosphorus (1.6) % for uncoated Ti alloy. Because the alloy is highly stable and bio-inert, especially after surface roughness to create nucleation sites that attract Ca and P ions from the fluid, and calcium (3.2) % as well as phosphorus (3.4) % for (PLA+9%CeO2). This development is attributed to the hydrophilic surface formed by the coating as shown in fig. 6 (a) and fig. 6(b), which, importantly, increases implant compatibility.

The results of contact angle test showed that the initial contact angle of the coated surfaces was always measured below 90°. Moreover, water droplets were observed to be absorbed and subsequently diffused throughout the coating layer across the entire specimen, indicating excellent wettability. Specifically, coatings containing ZrO_2 (15 wt.%) with an absorption rate around 61.061° and CeO_2 (15 wt.%) with an absorption rate about 63.428° compared with sample coated with pure PLA has an absorption rate about 68.531°.

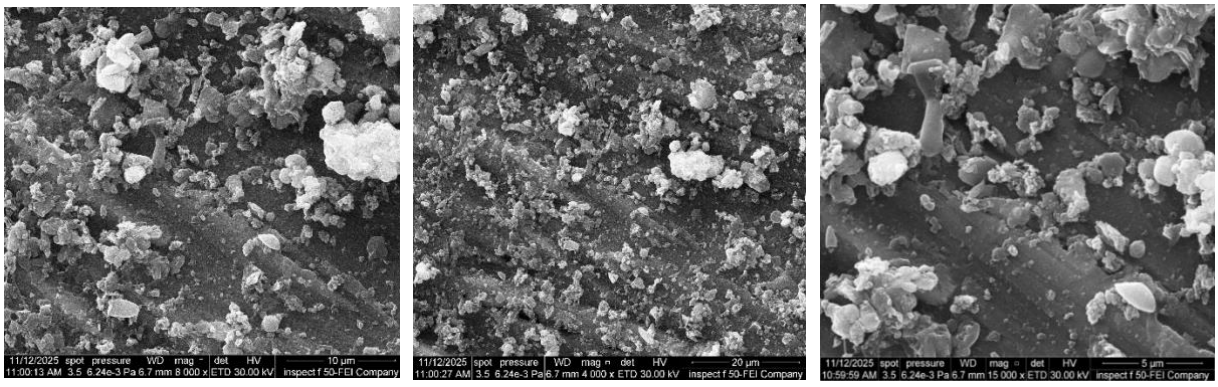

(a)

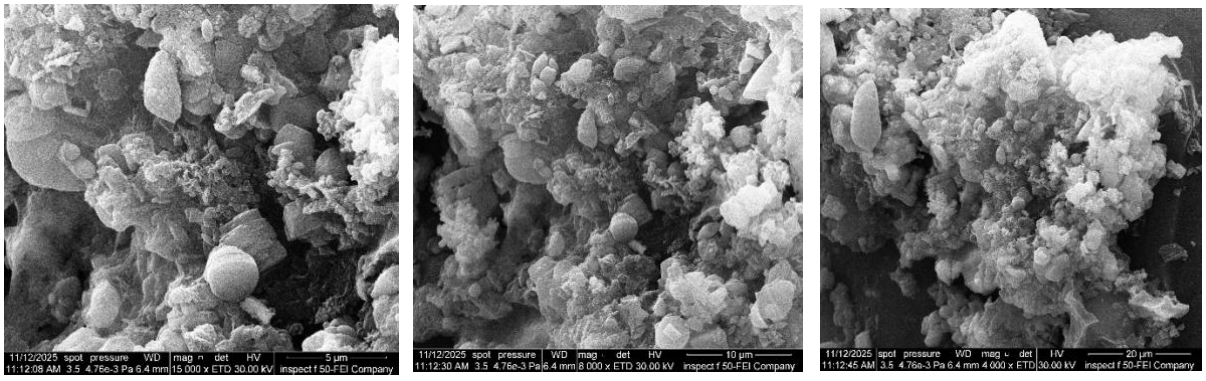

(b)

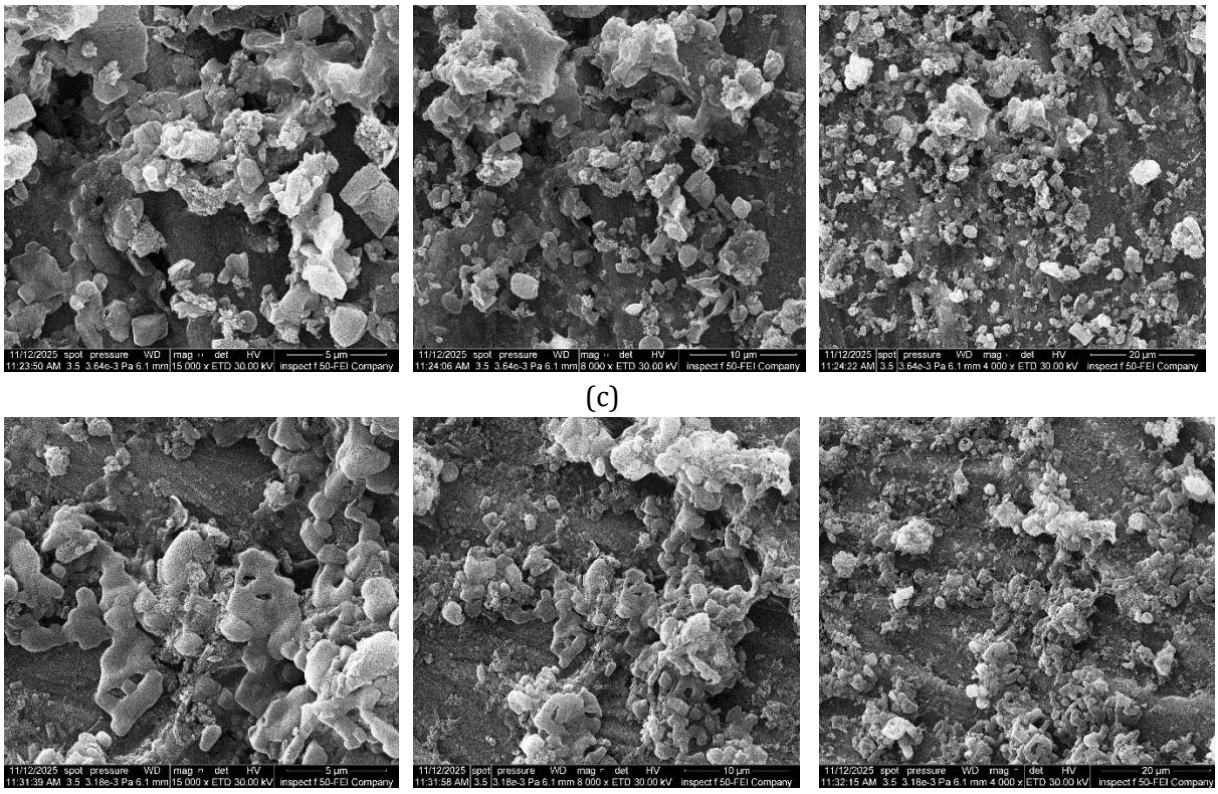

(c)

(d)

Fig. 4. FESEM of coated specimen after immersed in SBF solution of (a) Ti6Al4V alloy, (b) PLA, (c) PLA 9%ZrO2, (d) PLA+9%CeO2

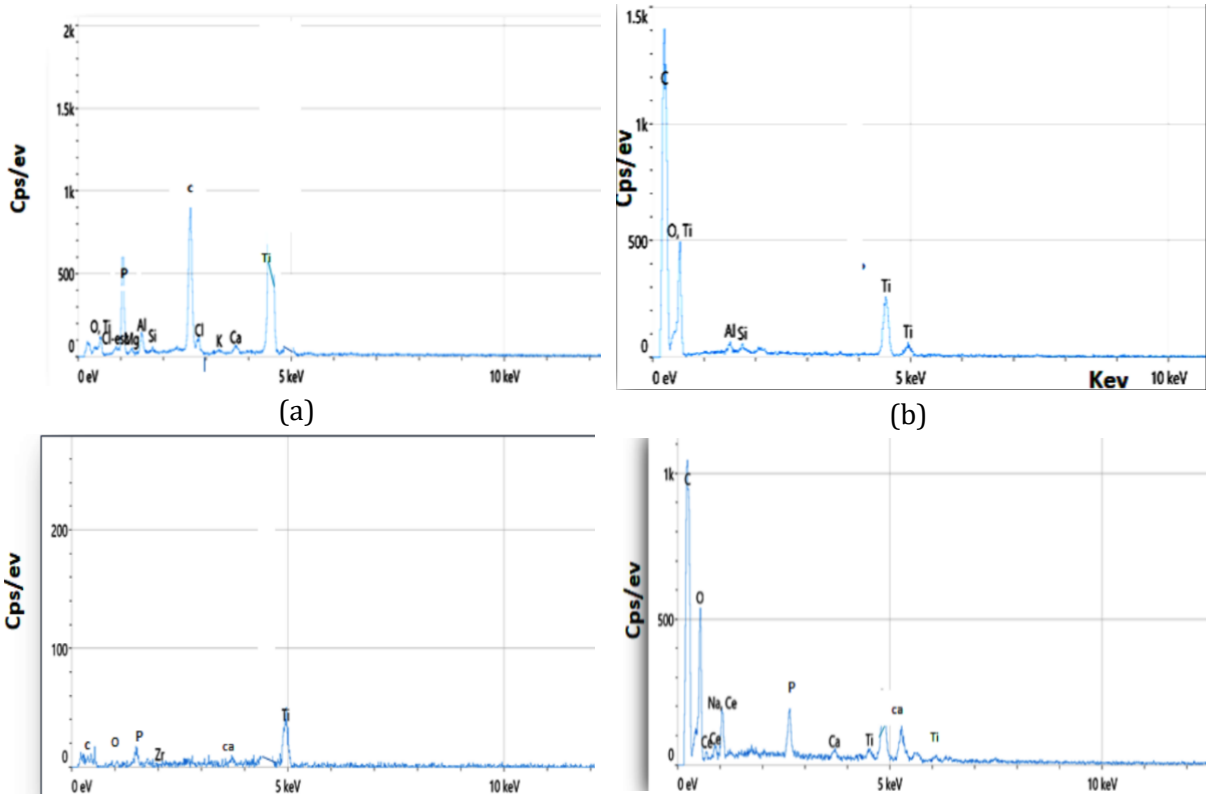

(a)

(b)

(c)

(d)

Fig. 5. EDS test of coated specimens after immersion in SBF solution (a)Ti6Al4V, (b)PLA, (c) PLA 9%ZrO_2, (d) PLA+9%CeO_2

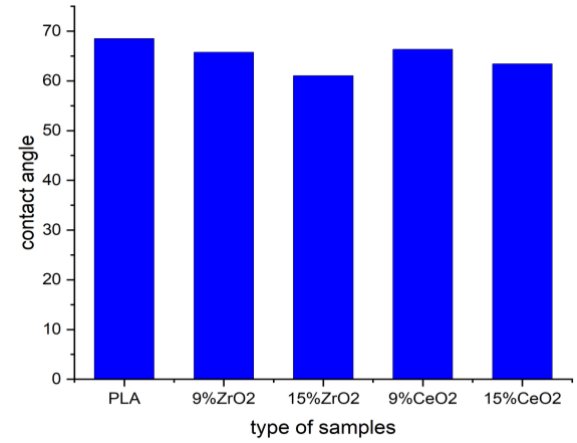

(a)

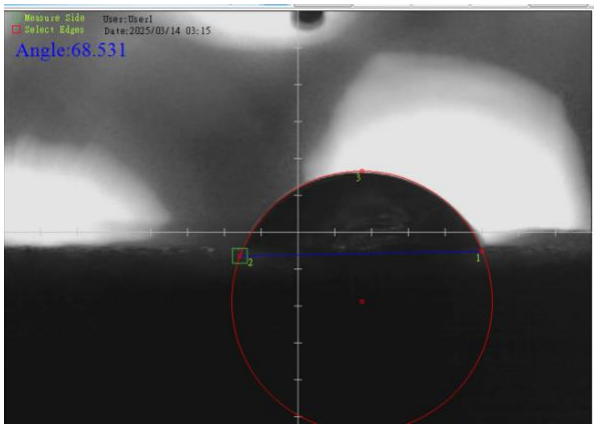

(b)

(c)

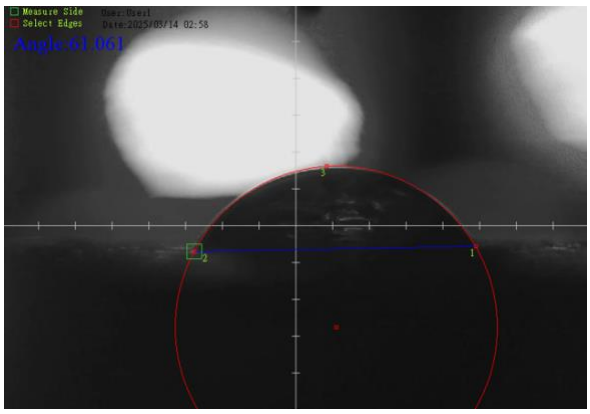

(d)

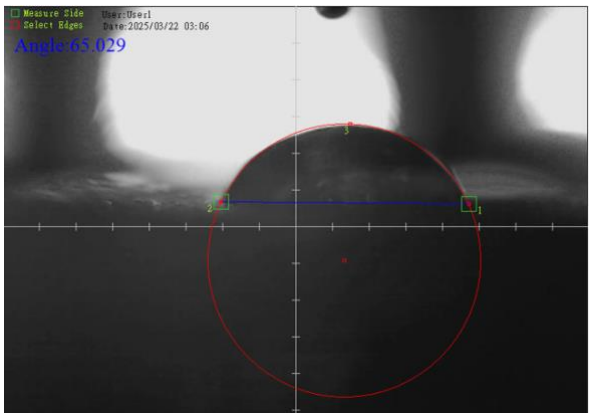

(e)

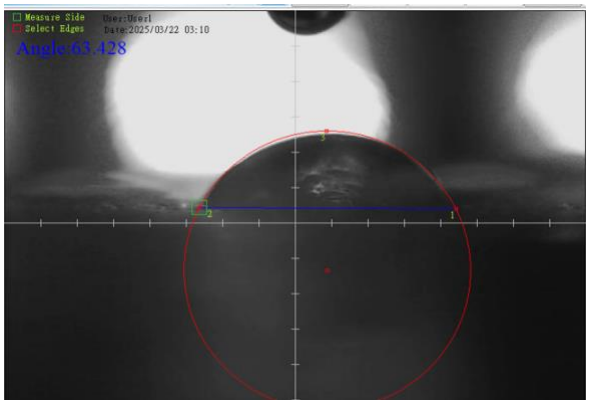

(f)

Fig. 6. (a) Contact Angle of coated samples, and samples of water droplet contact angles,(b)pure PLA,(c) PLA+9%ZrO_2 ,(d)PLA+ 15% ZrO_2 , (e)PLA+9CeO_2,(f) PLA+15%CeO_2

4.3 Hardness of Scratch

Scratch resistance, or hardness, is calculated by studying critical pressures, deformed volumes, and the deformation mechanisms that occur after the scratch test. Frequently, the assessment of sensitive loads throughout sequential scratch testing is achieved by integrating distortion-response data with an inspection of critical loads. The abrasion hardness order for PLA-based composites plus their coating layers is exhibited in Table 2 and Fig. 7. Scratch hardness can be determined utilizing the following equation:

$$Hsp = (4qP) / \pi W^2 \quad (1)$$

Where the Hsp: is the scratch hardness (N/mm^2), P: is the applied load (N), the factor q: is a mean value of (1.5) and W: indicating the actual scratch width after the test (μm).

The CeO2/PLA and ZrO2/PLA composite coatings show outstanding scratch resistance, attaining the highest scratch hardness values of 0.267 MPa and 0.221 MPa, respectively. Moreover, it exhibits the minimum average scratch width (0.55 and 0.5) μm, as depicted in table2. In contrast, the pure PLA coatings show higher average scratch widths, ranging from 1.07μm, with decreased scratch resistance strengths of 0.058 MPa. As shown in Fig. 7. The hardness of a coating's scratch is an important indicator of its adhesion properties. This is measured through analyzing microscope images of scratched coated samples. As shown in Fig.8, coatings with higher hardness exhibit the smallest scratch width, indicating the greatest level of adhesion. It is important to consider that many factors affect coating adhesion, including the applied force, coating thickness, and abrasion rate [26].

Table 2. The average width of a crack following a scratch

Type of specimens	Average crack width
PLA	1.07 μm
9%ZrO_2+PLA	0.79 μm
15%ZrO_2+PLA	0.55 μm
9%CeO_2+PLA	0.76 μm
15%CeO_2+PLA	0.5 μm

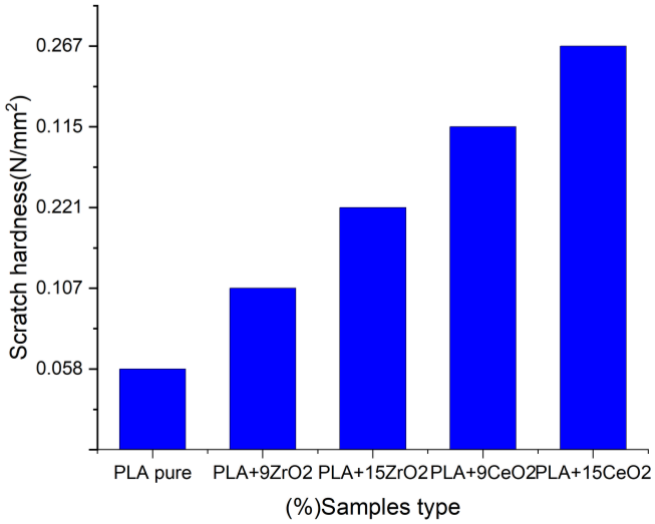

Fig. 7. Scratch hardness test of coated samples

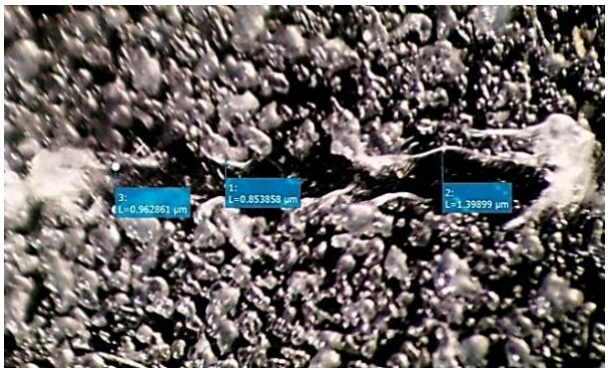

(a)

(b)

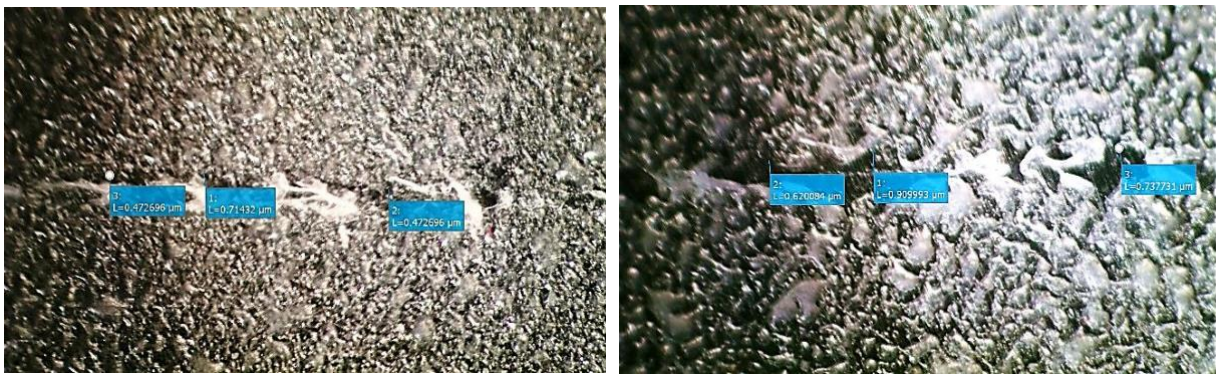

(c) (d)

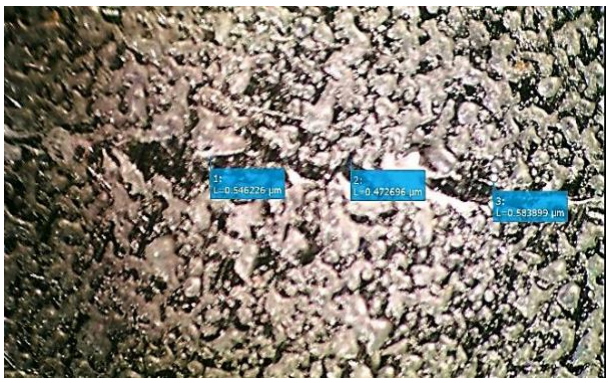

(e)

Fig. 8. Microscopic images for the scratch width for. (a) PLA Pure, (b) 9%ZrO_2+PLA, (c) 15%ZrO_2+PLA, (d) 9%CeO_2+PLA, (e) 15%CeO_2+PLA

4.4 Electrochemical Bio-Corrosion of Ti6Al4V Alloy and Coating Samples in SBF Solution.

4.4.1. Corrosion Resistance Analysis

Electrochemical corrosion examination was carried out utilizing a Corrtest CS350M Potentiostat/Galvanostat [27]. The pure and coated samples were cylindrical, with a diameter of 30 mm and a thickness of 3 mm. Each sample has been insulated with Bakelite, leaving only a circular surface exposed to simulated body fluid (SBF)at pH 7.4 [28]. A three-electrode cell configuration has been used to measure electrochemical reaction parameters. The setup involved a platinum electrode (the counter electrode, pure metal), a saturated calomel electrode (the reference), and Ti-based or coated samples as the working electrodes, have been wholly submerged in SBF solution. A water bath was working to keep a steady experimental temperature of 37 °C. The techniques done utilizing a Corrtest CS350M Potentiostat/Galvanostat workstation [29]. In this examination, a scan rate of 1 mV/s was used to generate Tafel plots (bc and ba), thereby allowing determination of the current density (icorr) and potential (Ecorr). Then, the corrosion rate (C.R.) was calculated using Equation (2) [30].

$$C.R. = C.(M/n\rho).icorr \quad (2)$$

where M: relates to the atomic weight (g/ mol), icorr: relates to current density (A/cm2), ρ: refers to density, C: relates to a constant equal to 0.00327 in (mm/y), and n: refers to the number of electrons included in the process.

4.4.2. Potentiodynamic Polarization Tests

The polarization examination curves for the studied samples are shown in Fig. 9 (a, b, c, and d). Key corrosion parameters, including corrosion potential (Ecorr), corrosion current density (Icorr), and corrosion rate (mm/y), were obtained from the polarization curves using the Tafel polarization

method. Figure 9 (a) explains the potentiodynamic polarization curve for the uncoated Ti6Al4V alloy, whereas Figure 9(b), 9(c), and9 (d) exhibit the coated alloy by pure PLA, (PLA + 9% ZrO_2), and (PLA + 9% CeO_2), respectively. In particular, both the corrosion current density and rate show a significant reduction when ceramic powders are added, with Icorr values becoming more negative. As detailed in Table 3, the corrosion rates (C.R.) of the coated specimens (b, c, d) are noted as 0.080027 mm/y, 0.001552 mm/y, and 1.901 x 10^-6 mm/y, respectively. These values are considerably lower than the corrosion rate of titanium alloy without a coating, which is 0.34109 mm/y.

Table 3. The parameters of corrosion for the examined samples

Samples groups	Ba (mv)	bc (mv)	I corr.(A/cm²) /10^{-6}	E corr.(v)	Corr. Rate (mm/y)
Ti6Al4V	450.83	370.35	$2.9075x10^{-5}$	-0.2455	0.064109
PLA Pure	50.196	37.432	$6.8218x10^{-6}$	-0.2375	0.080027
PLA+ 9% ZrO_2	49.664	39.66	$1.323x10^{-7}$	-0.18229	0.001552
PLA+9% CeO_2	54.9	39.79	$1.6205x10^{-10}$	-0.21589	$1.901x10^{-6}$

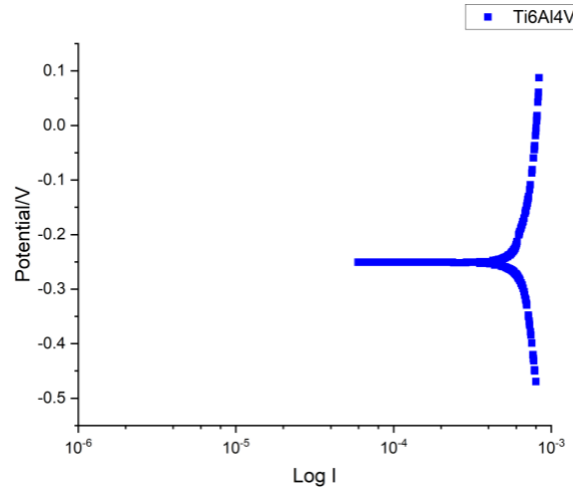

(a)

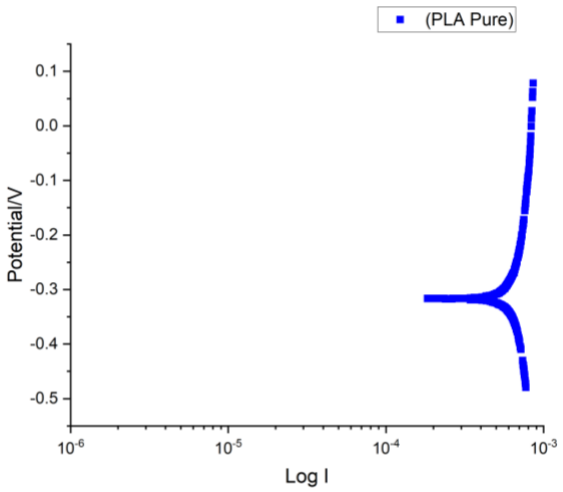

(b)

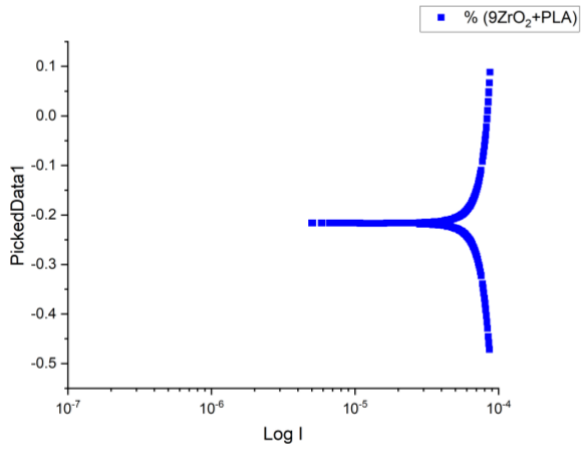

(c)

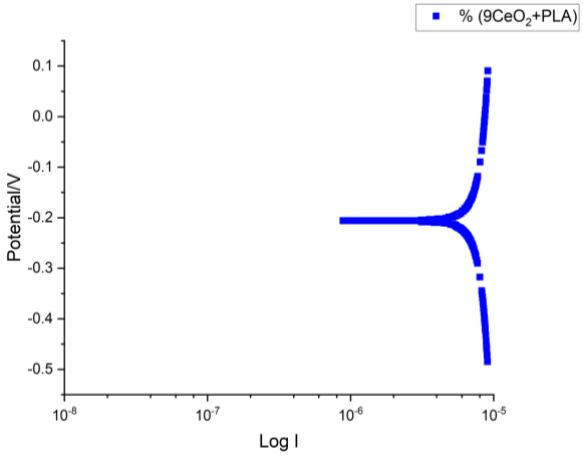

(d)

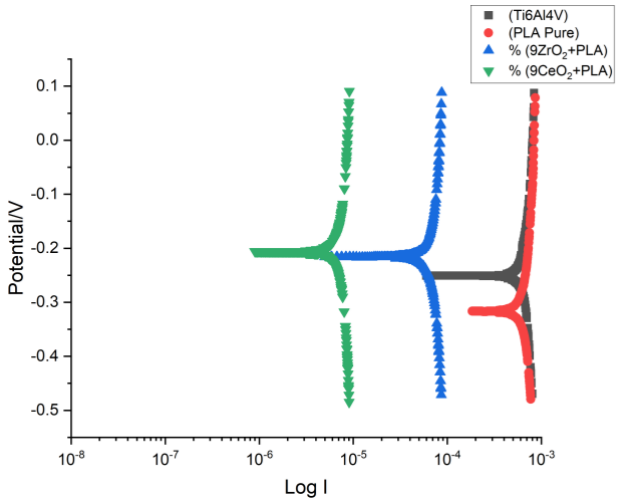

(e)

Fig. 9. Polarization curves of (a) uncoated Ti6Al4V alloy, (b) PLA Pure, (c) 9%ZrO_2+PLA, (d) 9%CeO_2+PLA and (e) all samples in SBF solution at 37ºC

5. Conclusions

The dry electrostatic deposition method was successfully employed to apply ZrO_2/PLA and CeO_2/PLA composites. SEM micrographs revealed a crack-free surface with a controlled level of porosity, which is beneficial for osseointegration. After 21 days of immersion in SBF at 37°C, the coated specimens showed a strong ability to form calcium (Ca) and phosphorus(P). The bio-composite coating (PLA+9%CeO_2) exhibits precipitation of calcium (3.2%) and phosphorus (3.4%) within the composite and groups, indicating the development of a strong and durable bond with surrounding bone tissues. Moreover, the scratch hardness of a coating is an essential indicator of adhesion, the highest scratch hardness was achieved with PLA+15%CeO_2 (0.5 µm scratch width), followed closely by PLA+15%ZrO_2(0.55 µm)."compared to pure PLA (1.07µm). These results highlight the improved biological compatibility of the coating layers within the body, in terms of corrosion resistance, (PLA+9%CeO_2) and (PLA+9%ZrO_2) showed the lowest corrosion rate ($1.901x10^{-6}$mm/y) and (0.001552 mm/y) respectively. These values are considerably lower than the corrosion rate of titanium alloy without a coating, which is 0.34109 mm/y. The study observed that ZrO_2 increased mechanical resistance by arresting crack propagation, while CeO_2 enhanced corrosion resistance by forming an ion barrier.

References

[1] Han Y, You X, Xing W, Zhang Z, Zou W. Paracrine and endocrine actions of bone: the functions of secretory proteins from osteoblasts, osteocytes, and osteoclasts. Bone Research. 2018;6:16. https://doi.org/10.1038/s41413-018-0019-6

[2] Harun WSW, Asri RIM, Alias J, Zulkifli FH, Kadirgama K, Ghani SAC, Shariffuddin JHM. A comprehensive review of hydroxyapatite-based coatings adhesion on metallic biomaterials. Ceramics International. 2018;44(11):1250-1268. https://doi.org/10.1016/j.ceramint.2017.10.162

[3] Sarker A, Tran N, Rifai A, Brandt M, Tran PA, Leary M, Fox K, Williams R. Rational Design of Additively Manufactured Ti6Al4V Implants to Control Staphylococcus aureus Biofilm Formation. Materialia. 2019;5:100250. https://doi.org/10.1016/j.mtla.2019.100250

[4] Tran PA, Sarker A, Tran N, Jeffery C, Rifai A, Fox K. Coatings on Metallic Implants for Biomedical Applications. Metallic Biomaterials Processing and Medical Device Manufacturing. 2020:359-385. https://doi.org/10.1016/B978-0-08-102965-7.00011-4

[5] Gepreel MAH, Niinomi M. Biocompatibility of Ti-alloys for long-term implantation. Journal of the Mechanical Behavior of Biomedical Materials. 2013;20:407-415. https://doi.org/10.1016/j.jmbbm.2012.11.014

[6] Anjaneyulu U, Priyadarshini B, Xavier SAS, Chellappa M, Geetha M, Vijayalakshmi U. Electrochemical behavior of laser shock peened Inconel 625 superalloy. Materials Technology. 2017;32(13):800-814. https://doi.org/10.1080/10667857.2017.1364476

[7] Xavier SSA, Karthick D, Swaroop S, KamachiMudali U, Vijayalakshmi U. Improved Biocompatible, Flexible Mesh Composites for Implant Applications via Hydroxyapatite Coating with Potential for 3-Dimensional Extracellular Matrix Network and Bone Regeneration. Ceramics International. 2018;44(3):3149-3160.
[8] Sivakumar T, Chandrasekaran K, Sridhar C, Tharanikumarm N. Titanium Alloys and Their Disadvantages in Medical and Dental Implants. IntechOpen; 2026. https://doi.org/10.5772/intechopen.1010633
[9] Wei G, Tan M, Attarilar S, Li J, Uglov VV, Wang B, Liu J, Wang L. An Overview of Surface Modification, A Way toward Fabrication of Nascent Biomedical Ti-6Al-4V Alloys. Journal of Materials Research and Technology. 2023;24:5896-5921. https://doi.org/10.1016/j.jmrt.2023.04.046
[10] Bahl S, Suwas S, Chatterjee K. Comprehensive review on alloy design, processing, and performance of β titanium alloys as biomedical materials. International Materials Reviews. 2021;66(2):114-139. https://doi.org/10.1080/09506608.2020.1735829
[11] Abar B, Kelly C, Pham A, Allen N, Barber H, Kelly A, Mirando AJ, Hilton MJ, Gall K, Adams SB. Effect of surface topography on in vitro osteoblast function and mechanical performance of 3D printed titanium. Journal of Biomedical Materials Research Part A. 2021;109(10):1792-1802. https://doi.org/10.1002/jbm.a.37172
[12] Younis S, Oleiwi JK, Mohammed RA. Some mechanical properties of polymer matrix composites reinforced by nano silica particles and glass fiber. Engineering and Technology Journal. 2018;36(12A):1283-1289. https://doi.org/10.30684/etj.36.12A.10
[13] Piszczek P, Radtke A, Ehlert M, Jędrzejewski T, Sznarkowska A, Sadowska B, Bartmański M, Erdoğan YK, Ercan B, Jędrzejczyk W. Comprehensive evaluation of the biological properties of surface-modified titanium alloy implants. Journal of Clinical Medicine. 2020;9(2):342. https://doi.org/10.3390/jcm9020342
[14] Ji Z, Wan Y, Zhao Z, Wang T, Yu M, Wang H, Fan S, Liu Z, Liu C. Polydopamine and magnesium ions loaded 3D-printed Ti-6Al-4V implants coating with enhanced osteogenesis and antibacterial abilities. Advanced Materials Technologies. 2022;7(11):2200598. https://doi.org/10.1002/admt.202200598
[15] Bernhardt A, Schneider J, Schroeder A, Papadopoulous K, Lopez E, Brückner F, Botzenhart U. Surface conditioning of additively manufactured titanium implants and its influence on materials properties and in vitro biocompatibility. Materials Science and Engineering C. 2021;119:111631. https://doi.org/10.1016/j.msec.2020.111631
[16] Chouirfa H, Bouloussa H, Migonney V, Falentin-Daudré C. Review of titanium surface modification techniques and coatings for antibacterial applications. Acta Biomaterialia. 2019;83:37-54. https://doi.org/10.1016/j.actbio.2018.10.036
[17] Zhao C, Zhu Y, Yuan Z, Li J. Structure and tribocorrosion behavior of Ti/TiN multilayer coatings in simulated body fluid by arc ion plating. Surface and Coatings Technology. 2020;403:126399. https://doi.org/10.1016/j.surfcoat.2020.126399
[18] Dhafer G, Al-Kaisy HA, Al-Shroofy MN. Fabrication of poly(methyl methacrylate)/hydroxyapatite composite coating over 316L stainless steel using electrostatic spray deposition. Advances in Mechanics. 2021;9(3):1156-1167.
[19] Bashar S, Al-Kaisy HA, Al-Shroofy MN. Characterization of the wettability of bio-composite coating on titanium alloy using electrostatic spray deposition. AIP Conference Proceedings. 2023;2830(1):030037. https://doi.org/10.1063/5.0157592
[20] Atay GY, Uslu G, Borras VA. Manufacturing antibacterial Ti-6Al-4V alloys using nano Ag particles synthesized by reduction method for biomedical applications. Discover Materials. 2024;4:64. https://doi.org/10.1007/s43939-024-00137-y
[21] Harb SV, Kolanthai E, Pugazhendhi AS, et al. 3D printed bioabsorbable composite scaffolds of poly (lactic acid)-tricalcium phosphate-ceria with osteogenic property for bone regeneration. Biomaterials and Biosystems. 2024;13:100086. https://doi.org/10.1016/j.bbiosy.2023.100086
[22] Yang Y, Weihua Z, Kunlong Z, Xiangyu S, Boxuan M, Yu S. Enhanced wear resistance, hydrophobic properties and corrosion resistance of plasma electrolyte oxidation coatings on Ti6Al4V alloys via addition of ZrO2 nanoparticles. Journal of Materials Research and Technology. 2025;34:463-478. https://doi.org/10.1016/j.jmrt.2024.12.053
[23] Roshan S, Sarabi AA. Improved performance of Ti-based conversion coating in the presence of Ce/Co ions: Surface characterization, electrochemical and adhesion study. Surface and Coatings Technology. 2021;410:126931. https://doi.org/10.1016/j.surfcoat.2021.126931
[24] Dhafer G, Al-Kaisy HA, Al-Shroofy MN. Electrostatic Deposition of Poly(Methyl Methacrylate)/Titanium Carbide Coatings on Austenitic 316L Stainless Steel Implant. Engineering and Technology Journal. 2022;40(06):918-925. https://doi.org/10.30684/etj.2022.131478.1038
[25] Jomaa DM, Hussien AK, Dawood JJ. Optimization of mechanical and biocompatible properties of ZnO fiber membranes. Engineering and Technology Journal. 2024;42(06):736-753. https://doi.org/10.30684/etj.2024.145042.1650

[26] Anaee RAM, Abdulmajeed MH. Tribocorrosion. Advances in Tribology. 2016;2016. (Not: Kitap bölümü veya spesifik bir makale ise sayfa/makale numarası eklenebilir). https://doi.org/10.5772/63657
[27] Naser SA, Anaee RA, Jaber HA, Khadom AA. Deposition of nickel-titanium coating on stainless steel 316L by direct current sputtering for bio-implants: electrochemical, microstructural, and morphological investigations. Inorganic Chemistry Communications. 2024;165:112478. https://doi.org/10.1016/j.inoche.2024.112478
[28] Ha H, Kim K, Park S, Lee T, Park H, Moon J, Hong H, Lee C. Effects of Cr on pitting corrosion resistance and passive film properties of austenitic Fe-19Mn-12Al-1.5C lightweight steel. Corrosion Science. 2022;206:110529. https://doi.org/10.1016/j.corsci.2022.110529
[29] Hadi M, Abdulkader NJ, Al-Gebory LW. Impact of sintering time on corrosion rate and relative density of titanium, titanium-aluminum alloy, and titanium-based composites for bio applications. Engineering and Technology Journal. 2025;43(07):1051-1065. https://doi.org/10.30684/etj.2025.156810.1886
[30] Azeez AA, Danyuo Y, Obayemi JD. Effect of particle size and sintering time on the mechanical properties of porous Ti-6Al-4V implant. SN Applied Sciences. 2020;2:819. https://doi.org/10.1007/s42452-020-2637-z